Journal of Advanced Ceramics

Volume 2 | Issue 4 Article 10

2013

Magnetic and structural properties of pure and Cr-doped haematite: α-$Fe_{2-x}Cr_xO_3$ ($0 \leq x \leq 1$)

Arvind YOGI
Materials Science Laboratory, School of Physics, Vigyan Bhawan, Devi Ahilya University, Khandwa Road Campus, Indore 452001, India School of Physics, Indian Institute of Science Education and Research, Thiruvananthapuram 695016, India

Dinesh VARSHNEY
Materials Science Laboratory, School of Physics, Vigyan Bhawan, Devi Ahilya University, Khandwa Road Campus, Indore 452001, India

Journal of Advanced Ceramics
2013, 2(4): 360–369
DOI: 10.1007/s40145-013-0084-7

ISSN 2226-4108
CN 10-1154/TQ

Research Article

Magnetic and structural properties of pure and Cr-doped haematite: α-$Fe_{2-x}Cr_xO_3$ ($0 \le x \le 1$)

Arvind YOGI[a,b], Dinesh VARSHNEY[a,*]

[a]*Materials Science Laboratory*, *School of Physics*, *Vigyan Bhawan*, *Devi Ahilya University*, *Khandwa Road Campus*, *Indore 452001*, *India*
[b]*School of Physics*, *Indian Institute of Science Education and Research*, *Thiruvananthapuram 695016*, *India*

Received: July 24, 2013; Revised: September 23, 2013; Accepted: October 13, 2013

Abstract: Solid-state ceramic technique route is used for synthesizing Cr-doped haematite α-$Fe_{2-x}Cr_xO_3$ ($x = 0$, 0.125, 0.50 and 1) samples. Single phase and corundum (Al_2O_3) type structure is revealed from the X-ray diffraction (XRD) patterns. The Raman spectra of α-$Fe_{2-x}Cr_xO_3$ illustrate seven phonon modes. On substitution of Cr ($x = 0$, 0.125, 0.50 and 1) at Fe site, all Raman active modes are shifted to higher wave numbers. The coercivity and remanence of Cr-doped haematites increase as x increases. The increased coercivity and remanence for Cr-doped samples can be attributed to their enhanced shape and magneto-crystalline anisotropy. The observed isomer shift δ values from room-temperature Mössbauer data clearly show the presence of ferric (Fe^{3+}) and Cr^{3+} ions illustrating strong ferromagnetic ordering up to $x = 0.125$ in α-$Fe_{2-x}Cr_xO_3$ haematite and weak ferromagnetic ordering for α-$Fe_{2-x}Cr_xO_3$ ($x > 0.125$) haematites.

Keywords: magnetic materials; X-ray diffraction (XRD); Raman spectra; Mössbauer spectroscopy

1 Introduction

Haematite, α-Fe_2O_3 is commonly described as rhombohedral or hexagonal with the space group $R\bar{3}c$ or D_{3d}^6, respectively. The structure of haematite is based on an arrangement of O^{2-} ions in a hexagonal close-packing, with Fe^{3+} ions being distributed in an ordered fashion in 2/3 of the octahedral sites. The crystal structure is the same as that of corundum, Al_2O_3. The framework of haematite is regarded as a set of O and Fe layers arranged in normal to three-fold axis, and the chains of face-sharing octahedra are directed along the *c*-axis, while the Fe^{3+} ions within each chain form pairs separated by an empty interstitial site. The magnetic structure of α-haematite was the subject of considerable discussion and debate in the 1950s, because it appeared to be ferromagnetic with Curie temperature of around 1000 K but with an extremely tiny moment ($0.002\mu_B$/Fe atom). Adding to the surprise was a transition to a phase with no net magnetic moment with a decrease in temperature at around 260 K (Morin transition) [1].

The substitution effect in α-Fe_2O_3 at Fe site influences the electrical, magnetic and other physical

* Corresponding author.
E-mail: vdinesh33@rediffmail.com

properties. The dopants used as substitution in α-Fe_2O_3 are Ti, Cr, Mn, Co, Ni, Cu, Zn, Al, Ga and Rh. The structural and magnetic properties of parent α-Fe_2O_3 are well established in the recent past; however, the doped α-Fe_2O_3 haematite leads to an increasing interest in the scientific community as the dopant like Zn ions substituting for Fe^{3+} in the corundum-related structure leads to formation of cationic and anionic vacancies [2–6]. The effect of substitution of Cr and Mn ions in $GaFeO_3$ manifests itself and can be delineated starting with suitable oxide precursors preferentially containing Cr (Mn) in the Ga or Fe site. It is noteworthy that Cr (Mn) substitution in the octahedral Fe (1,2) site of $GaFeO_3$ has marked effects on the structural parameters and magnetic properties, while substitution in the octahedral Ga 2 site has marginal effects [2–8]. The magnetic and structural properties of haematite are also affected by particle size [7,8], degree of crystallinity [9], pressure [10], doping [2–6], and mechanical alloying [11] due to its technological applications. It is noticed that depending upon milling conditions, structural phase transformations of nanostructured haematite to maghemite, magnetite and wüstite can be induced.

For identifying the vibrational phonon modes, Raman spectroscopy is a powerful probe. Raman measurements have been made at normal pressure and applying pressure for haematite (α-Fe_2O_3) as well [12]. The micro Raman spectra of Fe_2O_3 were measured at 62 GPa in a diamond anvil cell and at ambient conditions. The spectra depict all seven phonon (five E_g and two A_{1g}) modes predicted by group theory as $A_{1g}(1)$ (226 cm^{-1}), $E_g(1)$ (245 cm^{-1}), $E_g(2)$ (293 cm^{-1}), $E_g(3)$ (298 cm^{-1}), $E_g(4)$ (413 cm^{-1}), $A_{1g}(2)$ (500 cm^{-1}), and $E_g(5)$ (612 cm^{-1}) [13,14]. Apart from these modes, high-pressure spectra show an additional IR (infrared)-active E_u mode (~660 cm^{-1}) possibly induced by surface defects or stress. Furthermore, at high pressure, an additional Raman mode at 1320 cm^{-1} is observed and is attributed to a second order phonon–photon interaction. Earlier, McCarty has shown strong Raman features in $Fe_{2-x}Cr_xO_3$ at room temperature. The E_u mode (~660 cm^{-1}) of parent haematite varies linearly as a function of Cr doping and it is about 664 cm^{-1} for $Fe_{1.73}Cr_{0.27}O_3$ and 685 cm^{-1} for $Fe_{0.4}Cr_{1.6}O_3$, respectively [15,16]. McCarty and Boehme observed an additional band when chromium is substituted for iron in α-Fe_2O_3. The band ranges in Raman shift from 664 cm^{-1} for $Fe_{1.73}Cr_{0.27}O_3$ to 685 cm^{-1} for $Fe_{0.4}Cr_{1.6}O_3$, with the shift increasing nearly linearly with increasing chromium content [16].

The magnetic properties of haematite in bulk form and as spherical nanoparticles have been intensively studied because they have various applications in magnetic storage devices, spin electronic devices, drug delivery, tissue repair engineering, and magnetic resonance imaging [7,8,17–19]. In contrast to spherical nanoparticles, nanorods with their inherent one-dimensional (1-D) shape anisotropy may exhibit unique magnetic behavior, which is significantly different from that of the bulk material [20,21]. The magnetic properties of doped haematite are completely altered as compared to that of bulk haematite. However, few investigations of the magnetic properties of doped haematite have been reported [22,23].

Mössbauer spectroscopy is an impressive technique to probe the magnetic phases and to identify the magnetic ordering present in the structure as well. The parent haematite is paramagnetic above the Neel temperature ($T_N \approx 965$ K) and weakly ferromagnetic at room temperature, and at the Morin temperature ($T_M \approx 265$ K), it undergoes a phase transition to an antiferromagnetic state. The cation (Zn and Ni) substituted (5%) haematites show that T_M is essentially the same for both haematites and similar to that of undoped one. On the other hand, T_N is lower for the Ni-doped (5%) haematite ($\approx 883 \pm 2$ K) and Zn-doped (5%) haematite ($\approx 874 \pm 3$ K), and both are lower in comparison to T_N of single crystal haematite (965 K) [24]. Although the cation substitution suppresses T_N, an increase in T_M for Rh^{3+}, Ru^{3+} and Ir^{4+} is documented [25].

The room-temperature transmission Mössbauer spectra for parent haematite (α-Fe_2O_3) reveal magnetically resolved lines of haematite and are broadened progressively with increasing milling time (t_m). The static hyperfine field (B_{hf}) decreases from 51.5 T for non-milled sample down to 47 T for t_m = 2 h [26]. As far as cation substitution is concerned, the magnetic cation Cr and non-magnetic cation Ti doped haematites (α-Fe_2O_3) are the most studied ones. The Mössbauer spectrum of Cr-substituted haematite fitted using only single-sextet model at 200 K infers anti-ferromagnetic (AF) ordering; however, weak-ferromagnetic (WF) ordering is noticed at room temperature. On the other hand, the spectra fitted through two-sextet model at about 245 K show the coexistence of both the phases (AF and WF). The

magnetic hyperfine field (B_{hf}) for Cr-substituted Fe_2O_3 at AF (200 K) is B_{hf} = 54.45±0.01 T and it decreases (B_{hf} = 53.70±0.01 T) at WF (300 K) [27].

The near room-temperature Mössbauer spectra for $(Fe_{1-x}Ti_x)_2O_3$ ($x < 0.025$) fitted using single sextet of Lorentzian lines confirm the existence of WF phase. On the other hand, below 260 K, two sextets are essential for retracing the Mössbauer spectrum consisting of both WF and AF phases. The magnetic hyperfine field (B_{hf}) for Ti-doped haematite at 80 K results in B_{hf} = 52.7 T and B_{hf} = 53.5 T, respectively, while a reduced B_{hf} of about 51.0 T at 295 K with WF phase is documented [28]. On the other hand, non-magnetic cation as Zn-substituted haematites prepared by coprecipitation method is less studied and Zn^{2+}-doped haematites document an additional doublet pattern apart from single sextet and doublet. The hyperfine parameters are affected for Zn^{2+} substitution in haematites, and the decreasing magnetic ordering results in weak ferromagnetic nature [22].

In the present paper, we have prepared Cr^{3+}-doped α-$Fe_{2-x}Cr_xO_3$ haematites by solid-state ceramic technique route to seek the role of substitution (trivalent cation Cr^{3+} for trivalent Fe^{3+}) on the structural and magnetic properties following X-ray diffraction (XRD), Raman and Mössbauer spectroscopy. The immediate goal of the study is to see how the magnetic ordering changes with the impact of Cr^{3+} doping in α-Fe_2O_3.

2 Experimental techniques

2.1 Synthesis of samples

The polycrystalline samples with the composition α-$Fe_{2-x}Cr_xO_3$ (x = 0, 0.125, 0.50 and 1) were prepared by the solid-state ceramic technique route as described earlier [29]. Stoichiometry amounts for Fe_2O_3 and Cr_2O_3 were mixed and heated (calcinations) at different temperatures (850 ℃, 950 ℃ and 1050 ℃) in air for 24 h. After calcinations, we performed oxygen annealing at temperatures of 950 ℃ and 1050 ℃ for 24 h with intermediate grindings. The pellets were finally sintered and annealed at 1050 ℃ in oxygen atmosphere. All the samples were studied on a microscope slide as prepared and their structure were checked by XRD.

2.2 Characterization

2.2.1 X-ray diffraction

The XRD measurements were carried out with Cu Kα radiation using a Rigaku powder diffractometer which was equipped with a rotating anode scanning (0.01 (°)/step in 2θ) over the angular range of 10°–80° at room temperature and generating X-ray by 40 kV and 100 mA power settings. Monochromatic X-ray of λ = 1.5406 Å $K_{\alpha 1}$ line from a Cu target was made to fall on the prepared samples. The diffraction patterns were obtained by varying the scattering angle 2θ from 10° to 80° in step size of 0.01°.

2.2.2 Raman spectroscopy

The Raman equipment was a Jobin-Yovn Horiba Labram (System HR800) consisting of a single spectrograph (focal length 0.25 m) containing a holographic grating filter (1800 grooves/mm), and a Peltier-cooled CCD detector (1024 × 256 pixels of 26 μm). The spectra were excited with 632.8 nm radiation (1.95 eV) from a 19-mW air-cooled He–Ne laser (max laser power 19 mW) and the laser beam was focused on the sample by a 50× lens to give a spot size of 1 μm; the resolution was better than 2 cm^{-1}. The laser power was always kept on 5 mW at the samples to avoid sample degradation, except in the laser power dependence experiments. After each spectrum had been recorded, a careful visual inspection was performed using white light illumination on the microscope stage in order to detect any change that could have been caused by the laser.

2.2.3 Magnetization

The magnetization measurements on all the samples under investigation were performed using a vibrating sample magnetometer (VSM). Magnetic measurements for the samples in the powder form were carried out at room temperature using a VSM (Lakeshore 7300 model, USA). The hysteresis curves were obtained for the samples with different compositions. The applied field was varied from 0 to ±10 000 Oe, and from hysteresis curves representing the magnetization process at room temperature (300 K), the saturation magnetization (M_{sat}), remanent magnetization (M_r) and coercive force (H_c) have been determined.

2.2.4 Mössbauer spectroscopy

^{57}Fe Mössbauer measurements were performed in transmission mode with a ^{57}Co radioactive source in constant acceleration mode using a standard PC-based Mössbauer spectrometer equipped with a WissEl velocity drive. Velocity calibration of the spectrometer was done with a natural iron absorber at room temperature. High magnetic field ^{57}Fe Mössbauer measurements were carried out using a Janis superconducting magnet. For the high magnetic field measurements, the external field was applied parallel to the γ rays (i.e., longitudinal geometry). Absorbers were carefully prepared to optimize both a good compactness and an adequate heat transmission. Analysis of the spectra was performed using the NORMOS [30] least-squares fitting program. Doublets and sextets of Lorentzian lines were used, doublets in the paramagnetic region and sextets in the magnetic region. The spectra were calibrated referring to α-Fe.

3 Results and discussion

The XRD patterns have been collected on the surfaces of the disks with a Rigaku diffractometer using Cu Kα radiation. Figure 1 shows the representative 2θ scans of XRD for the parent and Cr^{3+}-substituted α-$Fe_{2-x}Cr_xO_3$ ($x=0$, 0.125, 0.50 and 1) haematites. Comparing the observed spectra with the standard diffraction pattern (JCPDS No. 86-0550), all Bragg peaks of the XRD patterns for the synthesized haematites in the doping range ($0 \leqslant x \leqslant 1$) are assigned to the presence of α-Fe_2O_3 phase and no other phase is identified. The XRD patterns for the α-$Fe_{2-x}Cr_xO_3$ are indexed as that of corundum type (α-Al_2O_3) structure at room temperature consistent with the earlier report [31]. In the XRD pattern for higher Cr doping, an additional Bragg peak is appeared at 2θ value of around 25.48°. The argument lies in a fact that iron oxides show multiple phases like haematite (α-Fe_2O_3), maghemite (γ-Fe_2O_3) and magnetite (Fe_3O_4). However, haematite (α-Fe_2O_3) is very sensitive with doping. For small Cr doping concentration, T_M changes and suppresses abruptly, and at higher Cr doping concentration, it completely disappears. The above is due to the variation of the charge concentration on Fe site [2–6]. Since powder XRD gives the average structural information and it is not a powerful tool for low doping concentration, we expect a change in XRD pattern. Thus, we observe an additional appearance of Bragg peak at around 25.48° in XRD pattern.

The Raman spectra of the Cr-doped α-$Fe_{2-x}Cr_xO_3$ ($x=0$, 0.125, 0.50 and 1) haematites in the range of 100 cm^{-1} to 800 cm^{-1} at room temperature and normal pressure are illustrated in Figs. 2 and 3. Figure 2 shows the Raman spectra of parent α-Fe_2O_3 and $Fe_{1.875}Cr_{0.125}O_3$ with seven phonon modes (two A_{1g} modes, five E_g modes and one Raman inactive or disorder E_u mode) predicted from the group analysis (Table 1) confirming corundum structure. For haematite α-Fe_2O_3, the phonon modes predicted by

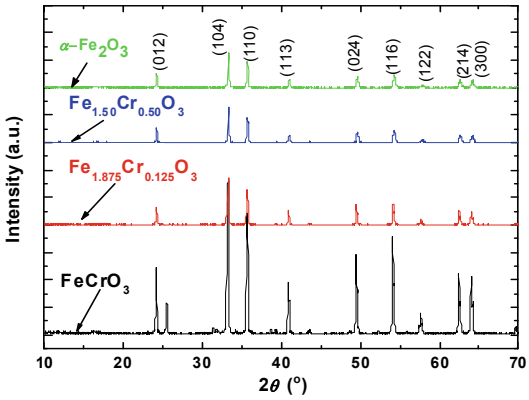

Fig. 1 The XRD patterns for α-$Fe_{2-x}Cr_xO_3$ ($x=0$, 0.125, 0.50 and 1).

Table 1 Raman shift (ν) and full width at half maximum (FWHM) (Γ) for haematite at a laser power of 5 mW

No.	Active mode	α-Fe_2O_3		$Fe_{1.875}Cr_{0.125}O_3$		$Fe_{1.50}Cr_{0.50}O_3$		$FeCrO_3$	
		ν (cm^{-1})	Γ (cm^{-1})	ν (cm^{-1})	Γ (cm^{-1})	ν (cm^{-1})	Γ (cm^{-1})	ν (cm^{-1})	Γ (cm^{-1})
1	$A_{1g}(1)$	225	5.6	226	5.7	227	5.9	229	6.1
2	$E_g(1)$	244	6.8	245	6.9	246	6.9	—	—
3	$E_g(2)$	292	7.6	292	7.6	293	8.1	285	28.2
4	$E_g(3)$	298	7.9	298	7.9	—	—	—	—
5	$E_g(4)$	410	13.1	412	13.6	413	15.1	401	18.1
6	$A_{1g}(2)$	496	20.6	498	20.8	500	21.1	504	25.3
7	$E_g(5)$	611	14.1	612	14.4	612	—	—	—
	E_u(disorder)	660	—	659	25.2	656	29.1	654	66.9

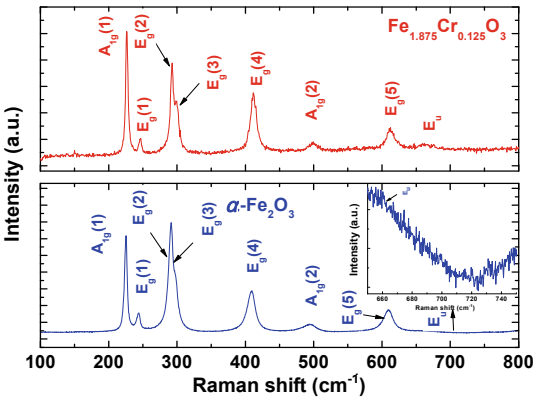

Fig. 2 Raman scattering intensities shown as a function of Raman shift (or wave number) for Fe_2O_3 and $Fe_{1.875}Cr_{0.125}O_3$. Inset shows the E_u mode for Fe_2O_3.

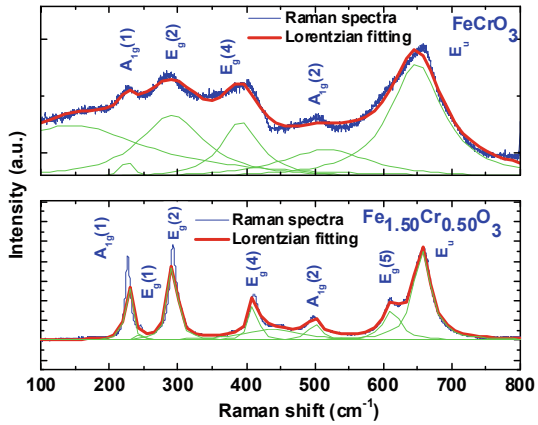

Fig. 3 Raman scattering intensities shown as a function of Raman shift (or wave number) for $Fe_{1.50}Cr_{0.50}O_3$ and $FeCrO_3$.

group theory are observed at $A_{1g}(1) \approx 225$ cm^{-1}, $E_g(1) \approx 244$ cm^{-1}, $E_g(2) \approx 292$ cm^{-1}, $E_g(3) \approx 298$ cm^{-1}, $E_g(4) \approx 410$ cm^{-1}, $A_{1g}(2) \approx 496$ cm^{-1}, and $E_g(5) \approx 611$ cm^{-1} consistent with the reported values in literatures [13,14]. It is noticed that the Raman spectrum in the range of 620–750 cm^{-1} shows an additional feature illustrating the Raman-inactive and IR-active E_u (LO) at about 660 cm^{-1} (the inset of Fig. 2).

On substitution of Cr ($x = 0$, 0.125) at Fe site, all seven phonon modes are observed and a small shift to higher wave numbers or Raman shift is seen in Fig. 2. The IR-active E_u (LO) (≈ 660 cm^{-1} for haematite (α-Fe_2O_3)) becomes sharp on Cr substitution and the FWHM (≈ 26 cm^{-1}) increases on enhancing the doping concentration. We note that IR-active E_u (LO) mode at 659 cm^{-1} is not group theoretically allowed in Raman spectrum. The sharp feature of E_u (LO) mode ($0.125 \leqslant x \leqslant 1$) at about 660 cm^{-1} is attributed to the possible disorder induced by Cr surface defects or stress. The E_u mode of parent haematite at 660 cm^{-1} decreases linearly as a function of Cr doping and it reaches at about 654 cm^{-1} for $x = 1$. On the other hand, the FWHM increases from 26 cm^{-1} to 67 cm^{-1} consistent with the earlier measurements [15].

The increase in FWHM (i.e., bandwidth, as shown in Table 1) might also arise from local heating due to the relatively high laser power (≈ 5 mW), which enhances anharmonic interactions. In present, the laser power is fixed to 5 mW (for all the samples) causing the bands to broaden and undergo a small shift to higher wave numbers or Raman shift, as illustrated in Table 1. Beattie and Gilbson argued that in α-Fe_2O_3 the bandwidth decreases and Fe band positions shift slightly to higher wave numbers at low temperature (77 K) [14]. This behavior seems to be fully reversible, as turning down the laser power causes the bandwidth to decrease.

In passing, we may refer to the work of McCarty and Boehme who observed an additional band when chromium is substituted for iron in α-Fe_2O_3. The band ranges in Raman shift from 664 cm^{-1} for $Fe_{1.73}Cr_{0.27}O_3$ to 685 cm^{-1} for $Fe_{0.4}Cr_{1.6}O_3$, with the shift increasing nearly linearly with increasing Cr content [16]. The present Raman spectrum changes gradually for Cr doping in α-$Fe_{2-x}Cr_xO_3$ ($x = 0$, 0.125, 0.50 and 1) which is attributed to the strong electron–phonon interaction in this system. The $E_g(3)$ mode is more pronounced for lower doping ($x = 0.125$), but for higher doping ($x > 0.125$), it does not document in the Raman spectra attributed to the fact that the non-magnetic ion Cr doping leads to structural changes in α-$Fe_{2-x}Cr_xO_3$ system. The 100% Cr^{3+} replacement by Fe ($FeCrO_3$) does not show three E_g modes in the Raman spectrum ($E_g(1)$, $E_g(3)$ or $E_g(5)$), while that the FWHM increases as Cr doping increases represented in Table 1 is consistent with earlier reported data [15,16].

Magnetic hysteresis measurements for Cr-doped bulk haematite α-$Fe_{2-x}Cr_xO_3$ ($x = 0$, 0.125, 0.50 and 1) were carried out in an applied magnetic field (H) at room temperature (300 K) as present in Figs. 4–7. The hysteresis loops of the Cr-doped α-Fe_2O_3 show a ferromagnetic behavior for all the prepared samples. Moreover, the magnetization measurements of parent and Cr-doped bulk haematites α-$Fe_{2-x}Cr_xO_3$ ($x = 0$, 0.125, 0.50 and 1) exhibit hysteretic features with

coercivity being determined to be 995 Oe, 1909 Oe, 2198 Oe and 3725 Oe, respectively (Figs. 4–7). The coercivity is an extrinsic property of a magnet, which depends not only on the spin carrier but also on the shape or size of the magnets [31,32]. The larger coercivity and remanence for Cr-doped samples can be attributed to their enhanced shape and magneto-crystalline anisotropy. The parent α-Fe_2O_3 shows the magnetic hysteresis loop at 300 K. We fail to observe saturation of the magnetization even under the maximum applied magnetic field of 10 kOe for all the prepared samples (Figs. 4–7). The parent α-Fe_2O_3 shows weak ferromagnetic behavior with the remanent magnetization (M_r) of 0.434 emu/g and coercivity (H_c) of 995 Oe. As increasing Cr doping concentration x in α-$Fe_{2-x}Cr_xO_3$ system, the coercivity and the remanence increase abruptly, which show ferromagnetic nature. These results are summarized in Table 2.

Hill *et al*. [21] observed the magnetic properties of bulk and mesoporous haematite (α-Fe_2O_3) at room temperature as well as at low temperature. For bulk α-Fe_2O_3, no hysteresis loop is observed at 12 K, in line with what is expected for a simple antiferromagnet. At 295 K, hysteresis is observed due to the weak ferromagnetic state of the material. Extrapolation of the high-field region of the $M(H)$ curve (where saturation occurs) provides a spontaneous magnetization, M_r, of 0.28 emu/g. At room temperature, however, the bulk material is a harder magnet than the

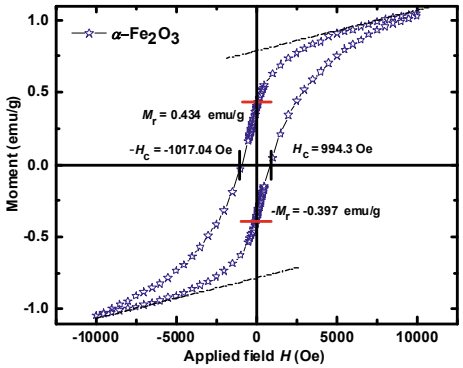

Fig. 4 Hysteresis loop for parent α-Fe_2O_3 sample at room temperature (300 K).

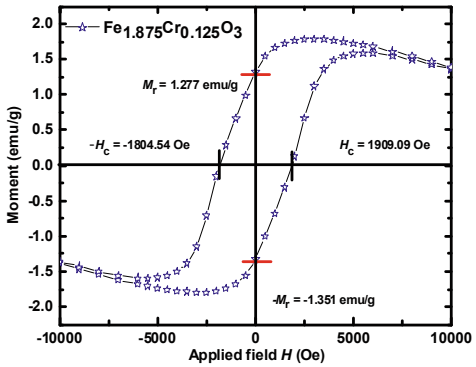

Fig. 5 Hysteresis loop for Cr-doped haematite α-$Fe_{1.875}Cr_{0.125}O_3$ sample at room temperature (300 K).

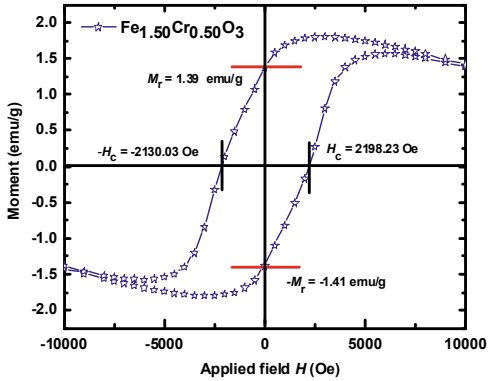

Fig. 6 Hysteresis loop for Cr-doped haematite α-$Fe_{1.50}Cr_{0.50}O_3$ sample at room temperature (300 K).

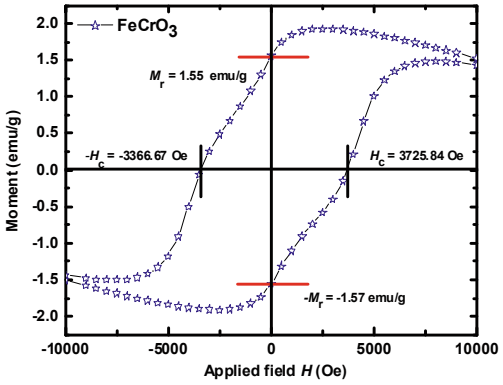

Fig. 7 Hysteresis loop for Cr-doped haematite α-$FeCrO_3$ sample at room temperature (300 K).

Table 2 Remanent magnetization (M_r) and coercive force (H_c) for Cr-doped α-$Fe_{2-x}Cr_xO_3$

Sample	Remnant magnetization, M_r (emu/g)	Coercive force, H_c (Oe)
Fe_2O_3	0.434	994.3
$Fe_{1.875}Cr_{0.125}O_3$	1.277	1909.1
$Fe_{1.50}Cr_{0.50}O_3$	1.390	2198.2
$FeCrO_3$	1.550	3725.8

mesoporous material, H_c = ~0.17 T. These results are higher in magnitude as compared to our results for parent α-Fe_2O_3, which may be due to the morphological difference. The effect of Co-coated haematite is studied and noticed that magnetic properties are changed with Co coating. According to the report, the coercivity of Co-coated haematite is higher than that of pure haematite by about 400 Oe [23]. In the present study of magnetization, the hysteretic features are changed gradually for Cr doping in α-$Fe_{2-x}Cr_xO_3$ (x = 0.125, 0.50 and 1) because magnetic properties are sensitive for doping concentration. It is well known that the magnetization of ferromagnetic materials is very sensitive to the morphology and structure of the as-synthesized sample. So the higher coercivity and remanent magnetization are due to the shape anisotropy of α-$Fe_{2-x}Cr_xO_3$ superstructures, which prevent them from magnetizing in directions other than along their easy magnetic axes, hence leading to the higher remanent magnetization and higher coercivity.

The ^{57}Fe Mössbauer spectra recorded at 300 K for Cr doping at Fe site α-$Fe_{2-x}Cr_xO_3$ (x = 0, 0.125, 0.50 and 1) are illustrated from Fig. 8 and Fig. 9, respectively. The Mössbauer spectra are analysed by considering single symmetric Lorentzian-shaped sextet model for parent (doped) haematites. The room-temperature Mössbauer spectra are fitted with NORMOS-SITE program [30] and all samples show strong magnetic ordering. The obtained value of chi-2 (χ^2) is minimum and NORMOS-SITE program is well fitted to the experimental data. The ^{57}Fe fitted Mössbauer parameters at room temperature are listed in Table 3. The Mössbauer parameters are derived from the spectra using the single symmetric Lorentzian-shaped sextet model, and an additional quadruple model is required for Cr doping (x > 0.50). The obtained hyperfine parameters are with respect to natural iron consistent with the earlier experimental data [22,26–28].

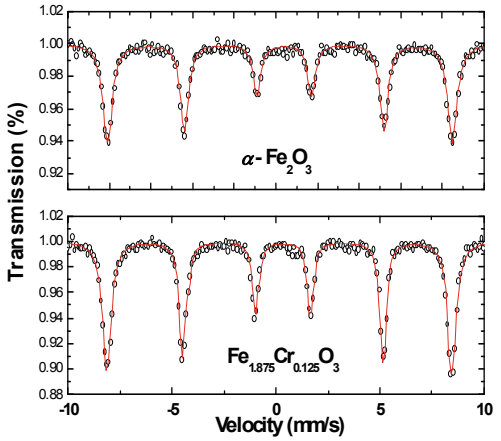

Fig. 8 Room-temperature Mössbauer spectra of the Fe_2O_3 and $Fe_{1.875}Cr_{0.125}O_3$ haematites.

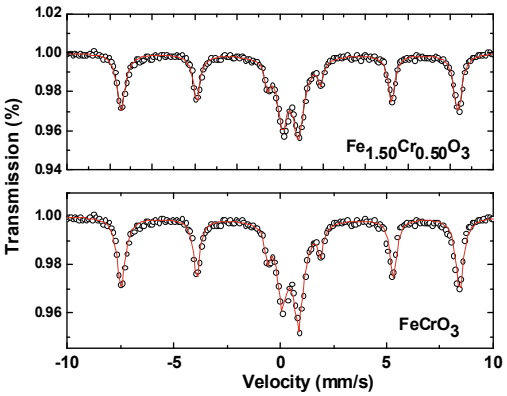

Fig. 9 Room-temperature Mössbauer spectra of the $Fe_{1.50}Cr_{0.50}O_3$ and $FeCrO_3$ haematites.

Table 3 ^{57}Fe Mössbauer parameters for Cr-doped α-Fe_2O_3

Sample	Assignment	δ (mm/s)	ΔE_Q (mm/s)	B_{hf} (T)	Relative area (%)
Fe_2O_3	Sextet	0.30	–0.15	51.18	100
$Fe_{1.875}Cr_{0.125}O_3$	Sextet	0.32	–0.19	52.0	100
$Fe_{1.50}Cr_{0.50}O_3$	Sextet	0.27	–0.21	50.9	76.93
	Doublet	0.24	0.38	—	23.07
$FeCrO_3$	Sextet	0.29	–0.23	49.7	75.18
	Doublet	0.26	0.36	—	24.82

Though α-Fe_2O_3 is a very common iron oxide in solids, it is particularly interesting due to its two magnetic phases namely week ferromagnetism (WF, at ambient condition, ~300 K) and antiferromagnetic (AF, at non-ambient condition, ~265 K). Due to its high Neel temperature (T_N = 965 K) and possibly a high effective anisotropy constant, the Mössbauer spectrum at room temperature appears as a sextet with a hyperfine field of about 51 T and a quadruple shift of about 0.2 mm/s. We have calculated these parameters using NORMOS-SITE program for all prepared samples, which are in good agreement with reported

results [22,24]. From these two results of α-Fe_2O_3 Mössbauer spectrum, one can be readily distinguished even at room temperature from other iron oxides, making again Mössbauer spectroscopy to be a powerful method for identification purposes.

From Fig. 8, the transmission Mössbauer spectroscopy of α-Fe_2O_3 reveals only single sextet indicating magnetically ordered state. The peaks with high hyperfine field values are related to the irons involved in the electron delocalization process, without the presence of Cr as the nearest neighbors. The transmission Mössbauer spectroscopy of α-$Fe_{2-x}Cr_xO_3$ ($0.50 \leqslant x \leqslant 1$) shows an additional peak corresponding to those iron atoms surrounded by Cr neighbors as depicted in Fig. 9. The additional feature is more pronounced for $x = 1$. It is noticed that the Fe site distributions become broader and occupy more area as the amount of Cr increases and the relative area decreases. The observed isomer shift values from room-temperature Mössbauer data clearly show the presence of ferric (Fe^{3+}) state and Cr is in Cr^{3+}. The negative values of the quadruple coupling constants (Table 3) for all Cr-doped haematites indicate that the material is weakly ferromagnetic at room temperature. This is mainly because the occupation of interstitial sites by Cr^{3+} ions replaces the vacancies on Fe^{3+} sites.

For undoped α-Fe_2O_3 we refer to our earlier work, where hyperfine field of about 51.18 T and a quadruple shift of about –0.15 mm/s are obtained [33]. Since Cr^{3+} shows low spin value (S = 3/2) and Fe^{3+} shows high spin value (S = 5/2), the difference in spin values of Cr^{3+} and Fe^{3+} ground state quantum fluctuations might be enhanced, which motivates us to perform Cr doping on this system. Because of the replacing of huge difference spin values, the Cr doping leads to the hyperfine field changing from 51.18 T to 49.7 T and the quadruple shift from –0.15 mm/s to –0.23 mm/s as a function of Cr doping at Fe site.

The room-temperature Mössbauer spectra of α-$Fe_{2-x}Cr_xO_3$ ($0.50 \leqslant x \leqslant 1$) haematites show an additional presence of a quadruple-split doublet [22,24]. The ^{57}Fe Mössbauer spectrum of $FeCrO_3$ recorded at 300 K (Fig. 9) shows the clear sextet pattern and a broad doublet. The doublet component value of isomer shift is $\delta = 0.26$ mm/s and the quadrupole is $\Delta E_Q = 0.36$ mm/s at 300 K. The NORMOS-SITE program fitting for Mössbauer spectrum of the magnetically split component of the $FeCrO_3$ spectrum to a single sextet yields a hyperfine magnetic field ($B_{hf} = 49.7 \pm 0.3$ T) smaller to that of pure α-Fe_2O_3 ($B_{hf} = 51.18 \pm 0.3$ T).

Furthermore, the linewidth of $FeCrO_3$ (0.32 mm/s) is an indicative of a distribution of sites originating from the presence of the dopant Cr^{3+} within the α-Fe_2O_3 structure. The spectrum is therefore fitted with sextet pattern and the field values (B_{hf}) are smaller for all Cr-doped haematites α-$Fe_{2-x}Cr_xO_3$. The above feature indicates that α-$Fe_{2-x}Cr_xO_3$ ($0.50 \leqslant x \leqslant 1$) is weakly ferromagnetic at room temperature as compared to the parent α-Fe_2O_3. In the α-Fe_2O_3 pattern the larger field ($B_{hf} = 51.18 \pm 0.3$ T) can be associated with Fe^{3+} ions which are not influenced by the presence of Cr, while in α-$Fe_{2-x}Cr_xO_3$ ($0.50 \leqslant x \leqslant 1$) the smaller field ($B_{hf} = 49.7 \pm 0.3$ T) can be assigned to Fe^{3+} ions that have Cr^{3+} ions in close proximity. The relative population of each magnetic component is varied with assumed linewidth without any significant change to the value of χ^2, and the percentage of Fe^{3+} influenced by Cr is therefore difficult to quantify.

4 Conclusions

The structural and magnetic ordering effects in polycrystalline α-$Fe_{2-x}Cr_xO_3$ ($0 \leqslant x \leqslant 1$) are studied by XRD, Raman spectra and Mössbauer spectroscopy. The crystal structure of the samples is studied using XRD. The XRD patterns identify the single phase and corundum or Al_2O_3 type structure of all the polycrystalline samples. The Raman spectra reveal seven Raman active modes (two A_{1g} modes, five E_g modes) and an additional Raman inactive E_u mode. The IR-active E_u (LO) (≈ 660 cm^{-1} for haematite (α-Fe_2O_3)) becomes sharp on Cr substitution, and the FWHM increases on enhancing the doping concentration (for 100% Cr doping, $\Gamma \approx 67$ cm^{-1}). The $E_g(3)$ mode is more pronounced for lower doping ($x = 0.125$), but for higher doping ($x > 0.125$) it does not document in the Raman spectra attributed to the fact that the non-magnetic ion Cr doping leads to structural changes in α-$Fe_{2-x}Cr_xO_3$ system. The 100% Cr^{3+} replacement of Fe ($FeCrO_3$) does not show three E_g modes in the Raman spectra ($E_g(1)$, $E_g(3)$ or $E_g(5)$) while the FWHM increases as Cr doping increases. Increase in Γ with Cr doping concentration is attributed to enhanced α-Fe_2O_3 bandwidth due to presence of Cr ion in the lattice and local heating by the relatively high laser power as well, which enhances

anharmonic interactions.

The coercivity and remanence of Cr-doped haematites increase as x increases. The coercivity H_c (remanence M_r) for $x=0$, 0.125, 0.50 and 1 is determined to be 995 Oe (0.44 emu/g), 1909 Oe (1.27 emu/g), 2198 Oe (1.39 emu/g) and 3725 Oe (1.55 emu/g), respectively. The larger coercivity and remanence for Cr-doped samples can be attributed to their enhanced shape and magneto-crystalline anisotropy. The room-temperature ^{57}Fe transmission Mössbauer spectroscopy of α-Fe_2O_3 reveals only single sextet indicating magnetically ordered state; however, a quadruple-split doublet is used for doped α-$Fe_{2-x}Cr_xO_3$ ($0.50 \leqslant x \leqslant 1$) implying weak magnetic ordering. The observed isomer shift δ values from room-temperature Mössbauer data clearly show the presence of ferric (Fe^{3+}) and Cr^{3+} ions illustrating strong ferromagnetic ordering up to $x=0.125$ in α-$Fe_{2-x}Cr_xO_3$ haematite and weak ferromagnetic ordering for α-$Fe_{2-x}Cr_xO_3$ ($x>0.125$) haematites.

Acknowledgements

Authors are thankful to UGC New Delhi for financial assistance and to UGC-DAE CSR, Indore for providing characterization facilities. Useful discussions with Dr. D. M. Phase, Dr. R. J. Choudhary, Dr. V. Sathe and Dr. V. R. Reddy are gratefully acknowledged.

References

[1] Saragovi C, Arpe J, Sileo E, *et al.* Changes in the structural and magnetic properties of Ni-substituted hematite prepared from metal oxinates. *Phys Chem Miner* 2004, **31**: 625–632.

[2] Van San E, De Grave E, Vandenberghe RE, *et al*. Study of Al-substituted hematites, prepared from thermal treatment of lepidocrocite. *Phys Chem Miner* 2001, **28**: 488–497.

[3] Kanai H, Mizutani H, Tanaka T, *et al*. X-ray absorption study on the local structures of fine particles of α-Fe_2O_3–SnO_2 gas sensors. *J Mater Chem* 1992, **2**: 703–707.

[4] Owoc D, Przewoznik J, Kozlowski A, *et al*. X-ray studies of $Fe_{3-x}Me_xO_4$, Me = Zn, Ti and Al; the impact of doping on the Verwey transition. *Physica B* 2005, **359–361**: 1339–1341.

[5] Busca G, Ramis G, Prieto MC, *et al*. Preparation and characterization of $Fe_{2-x}Cr_xO_3$ mixed oxide powders. *J Mater Chem* 1993, **3**: 665–673.

[6] Musić S, Lenglet M, Popović S, *et al*. Formation and characterization of the solid solutions $(Cr_xFe_{1-x})_2O_3$, $0 \leqslant x \leqslant 1$. *J Mater Sci* 1996, **31**: 4067–4076.

[7] Zysler RD, Fiorani D, Testa AM, *et al*. Size dependence of the spin-flop transition in hematite nanoparticles. *Phys Rev B* 2003, **68**: 212408.

[8] López JL, Pfannes H-D, Paniago R, *et al*. Investigation of the static and dynamic magnetic properties of $CoFe_2O_4$ nanoparticles. *J Magn Magn Mater* 2008, **320**: e327–e330.

[9] Dang M-Z, Rancourt DG, Dutrizac JE, *et al*. Interplay of surface conditions, particle size, stoichiometry, cell parameters, and magnetism in synthetic hematite-like materials. *Hyperfine Interact* 1998, **117**: 271–319.

[10] Bruzzone CL, Ingalls R. Mössbauer-effect study of the Morin transition and atomic positions in hematite under pressure. *Phys Rev B* 1983, **28**: 2430–2440.

[11] Hofmann M, Campbell SJ, Kaczmarek WA, *et al*. Mechanochemical transformation of α-Fe_2O_3 to $Fe_{3-x}O_4$—Microstructural investigation. *J Alloys Compd* 2003, **348**: 278–284.

[12] Bersani D, Lottici PP, Montenero A. Micro-Raman investigation of iron oxide films and powders produced by sol–gel syntheses. *J Raman Spectrosc* 1999, **30**: 355–360.

[13] Shim S-H, Duffy TS. Raman spectroscopy of Fe_2O_3 to 62 GPa. *Am Mineral* 2001, **87**: 318–326.

[14] Beattie IR, Gilson TR. The single-crystal Raman spectra of nearly opaque materials. Iron(III) oxide and chromium(III) oxide. *J Chem Soc A* 1970: 980–986.

[15] McCarty KF. Inelastic light scattering in α-Fe_2O_3: Phonon vs magnon scattering. *Solid State Commun* 1988, **68**: 799–802.

[16] McCarty KF, Boehme DR. A Raman study of the systems $Fe_{3-x}Cr_xO_4$ and $Fe_{2-x}Cr_xO_3$. *J Solid State Chem* 1989, **79**: 19–27.

[17] Zhao Y, Dunnill CW, Zhu Y, *et al*. Low-temperature magnetic properties of hematite nanorods. *Chem Mater* 2007, **19**: 916–921.

[18] Bødker F, Hansen MF, Koch CB, *et al*. Magnetic properties of hematite nanoparticles. *Phys Rev B* 2000, **61**: 6826–6838.

[19] Rath C, Sahu KK, Kulkarmi SD, *et al*.

Microstructure-dependent coercivity in monodispersed hematite particles. *Appl Phys Lett* 1999, **75**: 4171.

[20] Gregg KA, Perera SC, Lawes G, *et al*. Controlled synthesis of MnP nanorods: Effect of shape anisotropy on magnetization. *Chem Mater* 2006, **18**: 879–886.

[21] Hill AH, Jiao F, Bruce PG, *et al*. Neutron diffraction study of mesoporous and bulk hematite, α-Fe_2O_3. *Chem Mater* 2008, **20**: 4891–4899.

[22] Ayub I, Berry FJ, Bilsborrow RL, *et al*. Influence of zinc doping on the structural and magnetic properties of α-Fe_2O_3. *J Solid State Chem* 2001, **156**: 408–414.

[23] He T, Luo H-L, Li S. Effect of cobalt on the morin transition of hematite. *J Magn Magn Mater* 1988, **71**: 323–328.

[24] Barrero CA, Arpe J, Sileo E, *et al*. Ni- and Zn-doped hematite obtained by combustion of mixed metal oxinates. *Physica B* 2004, **354**: 27–34.

[25] Morrish AH. *Canted Antiferromagnetism*: *Hematite*. Singapore: World Scientific Publishing Company, 1994.

[26] Stewart SJ, Borzi RA, Cabanillas ED, *et al*. Effects of milling-induced disorder on the lattice parameters and magnetic properties of hematite. *J Magn Magn Mater* 2003, **260**: 447–454.

[27] Sileo EE, Daroca DP, Barrero CA, *et al*. Influence of the genesis on the structural and hyperfine properties of Cr-substituted hematites. *Chem Geol* 2007, **238**: 84–93.

[28] Ericsson T, Krisnhamurthy A, Srivastava BK. Morin-transition in Ti-substituted hematite: A Mössbauer study. *Phys Scr* 1986, **33**: 88.

[29] Varshney D, Yogi A. Structural and transport properties of stoichiometric and Cu^{2+}-doped magnetite: $Fe_{3-x}Cu_xO_4$. *Mater Chem Phys* 2010, **123**: 434–438.

[30] Ruebenbauer K, Birchall T. A computer programme for the evaluation of Mössbauer data. *Hyperfine Interact* 1979, **7**: 125–133.

[31] Li L, Chu Y, Liu Y. Synthesis and characterization of ring-like α-Fe_2O_3. *Nanotechnology* 2007, **18**: 105603.

[32] Jacob J, Abdul Khadar M. VSM and Mössbauer study of nanostructured hematite. *J Magn Magn Mater* 2010, **322**: 614–621.

[33] Varshney D, Yogi A. Structural and electrical conductivity of Mn doped hematite (α-Fe_2O_3) phase. *J Mol Struct* 2011, **995**: 157–162.